Spatial bias in field-estimated unsaturated hydraulic properties

Robert M. Holt

Department of Geology and Geological Engineering, University of Mississippi, University, Mississippi, USA

John L. Wilson

Department of Earth and Environmental Sciences, New Mexico Institute of Mining and Technology, Socorro, New Mexico, USA

Robert J. Glass

Flow Visualization and Processes Laboratory, Sandia National Laboratories, Albuquerque, New Mexico, USA

Received 28 March 2002; revised 15 April 2002; accepted 19 April 2002; published 20 December 2002.

[1] We use a Monte Carlo approach to explore the potential impact of observation and inversion model errors on the spatial statistics of field-estimated unsaturated hydraulic properties. For this analysis we simulate tension infiltrometer measurements in a series of idealized realities, each consisting of spatially correlated random property fields. We consider only simple measurement errors that can be easily modeled. We show that estimated hydraulic properties are strongly biased by small, simple observation and inversion model errors. This bias can lead to order-of-magnitude errors in spatial statistics and artificial cross correlation between measured properties. The magnitude of bias varies with the true mean of the property field, the type of error considered, and the type of spatial statistic. We find no unique indicators of bias as property values may appear reasonable and spatial statistics may look realistic. Our results suggest new concerns for geostatisticians, stochastic modelers, and unsaturated zone practitioners who are unaware of the potential impact of spatial bias in field-estimated properties. *INDEX TERMS:* 1869 Hydrology: Stochastic processes; 1875 Hydrology: Unsaturated zone; 1829 Hydrology: Groundwater hydrology; 1894 Hydrology: Instruments and techniques; 5114 Physical Properties of Rocks: Permeability and porosity; *KEYWORDS:* unsaturated zone, geostatistics, spatial bias, measurement error, inversion model error, hydraulic property measurement

Citation: Holt, R. M., J. L. Wilson, and R. J. Glass, Spatial bias in field-estimated unsaturated hydraulic properties, *Water Resour. Res.*, *38*(12), 1311, doi:10.1029/2002WR001336, 2002.

1. Introduction

[2] In recent years, there has been an increased focus on characterizing the spatial variability of unsaturated hydraulic properties. A variety of field methods for estimating *in situ* hydraulic properties have been developed [e.g., *Reynolds and Elrick*, 1987; *Ankeny et al.*, 1991; *Simunek and van Genuchten*, 1996] and applied in spatial variability studies [e.g., *Istok et al.*, 1994; *Jarvis and Messing*, 1995; *Mohanty et al.*, 1994; *Russo et al.*, 1997; *Shouse and Mohanty*, 1998]. Although most studies carefully document instrument procedures, the magnitude of errors in hydraulic property estimates and their impact on spatial statistics determined from field data remain unevaluated.

[3] Many estimated hydraulic properties (e.g., hydraulic conductivity) are likely to contain systematic error, or bias, because they are not measured directly. In a typical property measurement (e.g., pumping or permeameter test), a boundary condition is imposed on the hydraulic system, and the response of the system to that perturbation is monitored. Properties are then estimated indirectly using nonlinear, analytical or numerical, inversion models to infer property values from the observed responses and boundary conditions. Because property estimates depend on nonlinear inversion models, purely random error in the observations (observation error) can lead to spatially-correlated, systematic error, or bias, in the derived property value [*Mandel*, 1964]. Spatial bias may also result when the inversion model (e.g., governing equations, boundary conditions, initial conditions, constitutive models, etc.) is inadequate (inversion model error) [*Kempthorne and Allmaras*, 1986].

[4] In this paper, we develop and apply a Monte Carlo approach to explore the relationship between observation and inversion model errors and the resulting bias in the spatial statistics of field-estimated unsaturated hydraulic properties. We conduct Monte Carlo error analyses across a series of simplified artificial realities, where constitutive relationships are completely known. The mean values of hydraulic properties are varied between realities to define a parameter space and reveal the relationship between the true hydraulic properties and spatial bias. For each artificial reality, we generate a spatially correlated random field of the saturated hydraulic conductivity and the exponential relative permeability parameter [*Gardner*, 1958]. We then re-estimate these properties using simulated tension infiltrometer measurements subject to known random errors. For this illustration, we limited the number of errors to two types of observation error (both related to transducer error) and one type of inversion model error. The spatial statistics of the estimated properties are compared to those of the true properties to assess bias. To

0043-1397/02/2002WR001336$09.00

ensure that bias reflects only property-measurement errors, we sample all locations in a reality, eliminating errors in spatial statistics due to sampling design.

[5] We find that small, simple observation and inversion model errors can lead to significant bias in spatial statistics of field-estimated properties. Some statistics (e.g., the mean and variogram model parameters) can show an order of magnitude error in some parts of our parameter space. Bias is not homogeneous and varies with the true mean of the property field, the type of error considered, and the type of spatial statistic. We also see that observation and inversion model errors can lead to strong cross correlation between estimated parameters, even when there is none. We observe no unique indicators of spatial bias, as biased statistics can appear realistic and reasonable.

2. Methods

[6] We assume that Richard's equation is valid and that the unsaturated hydraulic conductivity is completely described by the *Gardner* [1958] parametric model

$$K(\psi) = K_s \exp(-\alpha\psi) \tag{1}$$

where ψ is the tension or the absolute value of the matric potential, α is the slope of $\ln[K(\psi)]/\psi$, and K_s is the saturated hydraulic conductivity. We also assume that $\ln(\alpha)$ and $\ln(K_s)$ are second-order stationary, isotropic random fields completely described by their mean values and a 2D, isotropic, exponential variogram model

$$\gamma^e(\mathbf{h}) = \sigma^2\left[1 - \exp\left(-\frac{\mathbf{h}}{\lambda_c}\right)\right] \tag{2}$$

where σ^2 is the variance of the random process, $\mathbf{h}$ is a separation vector, and λ_c is the correlation length. We generate 221 pairs of spatially correlated $\ln(\alpha)$ and $\ln(K_s)$ fields, with $\mathrm{cov}[\ln(\alpha), \ln(K_s)] = 0$, and vary the geometric means of α and K_s between pairs. Each pair of $\ln(\alpha)$ and $\ln(K_s)$ fields constitutes an artificial reality. At every spatial location in a reality, we simulate two steady state tension infiltrometer measurements, subject to simple errors, using the analytical approximation of *Wooding* [1968]. We assume that *Wooding*'s [1968] approximation is exact and that no sub-sample-scale heterogeneity exists. Then we re-estimate α and K_s using the experimental method of *Reynolds and Elrick* [1991]. We calculate the spatial statistics of the estimated fields of $\ln(\alpha)$ and $\ln(K_s)$ and compare their values with the known, "true" field statistics. Relevant details are discussed below.

2.1. Random Fields

[7] For each reality we generate over 262,000 pairs (a 512×512 random field) of lognormal α and K_s with a fixed geometric mean and variance. The pore size parameter, α, is typically assumed to follow a normal distribution in most unsaturated stochastic models [e.g., *Yeh et al.*, 1985a, 1985b, 1985c; *Mantoglou and Gelhar*, 1987a, 1987b; *Indelman et al.*, 1993; *Zhang et al.*, 1998]. However, we have chosen to describe α with a lognormal distribution because a lognormal distribution may be more realistic [e.g., *White and Sully*, 1992; *Russo et al.*, 1997].

[8] The geometric means of α and K_s (α^G and K_s^G respectively) are varied between realities to define a parameter space representative of poorly sorted to well-sorted silt to coarse sand. *Philip* [1969] suggests that the parameter α ranges between 0.002 to 0.05 cm^{-1}, although other reported values are both smaller than 0.002 cm^{-1} [e.g., *Bresler*, 1978; *Russo and Bouton*, 1992] and greater than 0.05 cm^{-1} [e.g., *Clothier et al.*, 1985; *Russo et al.*, 1997]. α^G is varied from 10^{-4} to 0.1 cm^{-1} to encompass this range of values. Similarly, we vary K_s^G from 10^{-5} cm/s to 0.1 cm/s. This range is consistent with the range of hydraulic conductivity values reported in tension infiltrometer studies [e.g., *Ankeny et al.*, 1991; *Hussen and Warrick*, 1993; *Shouse and Mohanty*, 1998] and is representative of silty sand to coarse sand [e.g., *Freeze and Cherry*, 1979]. Across our entire parameter space, we generate $13 \times 17 = 221$ pairs of random fields, in which the means of $\ln(K_s)$ and $\ln(\alpha)$ are each incremented by steps of size 0.576 between simulations.

[9] The variances of $\ln(\alpha)$ and $\ln(K_s)$ remain arbitrarily fixed at 1.0 which are consistent with the range of values reported from field studies [e.g., *Russo and Bouton*, 1992; *Mohanty et al.*, 1994; *Istok et al.*, 1994; *Russo et al.*, 1997]. We assume that the spatial structure of the random fields is statistically isotropic and completely described by an exponential variogram (2). In stochastic models, it is often assumed that the correlation lengths of unsaturated parameters are the same [e.g., *Yeh et al.*, 1985a, 1985b, 1985c; *Mantoglou and Gelhar*, 1987a, 1987b], and for convenience, we set all correlation lengths equal to 10 length units. Random fields are generated using the FFT method [e.g., *Robin et al.*, 1993].

2.2. Tension Infiltrometer Background

[10] We simulate tension infiltrometer measurements in the presence of simple errors to provide estimates of α and K_s. The tension infiltrometer is an instrument commonly used for examining the spatial variability of unsaturated hydraulic properties [e.g., *U.S. Department of Energy* (*U.S. DOE*), 1993; *Mohanty et al.*, 1994; *Jarvis and Messing*, 1995; *Shouse and Mohanty*, 1998]. It is a simple device for applying a constant (negative) pressure boundary condition to unsaturated soil (Figure 1). Contact with the soil is established using a porous membrane on the base plate ring. Typically, a ring is placed on the soil surface and filled with fine sand. The base plate is placed upon the sand, which provides improved contact with the soil. Flow from the instrument is induced by a capillary gradient. The flux from the instrument is determined by monitoring the declining water level in the Mariotte bottle (Figure 1). The design and typical operation of the tension infiltrometer is described by *Ankeny et al.* [1988]. With knowledge of two applied pressures and corresponding observed steady state flux rates, parameters α and K_s can be estimated using the analytical approximation of *Wooding* [1968].

2.3. Tension Infiltrometer Errors

[11] For this illustration we limit the number of tension infiltrometer errors and consider only two error scenarios. In the first, pressure transducer errors (there are two transducers used to estimate the tension infiltrometer flux rate and one transducer used to estimate the applied pressure at the disk source) yield errors in observations of flux rates and applied pressures. The second scenario includes these two

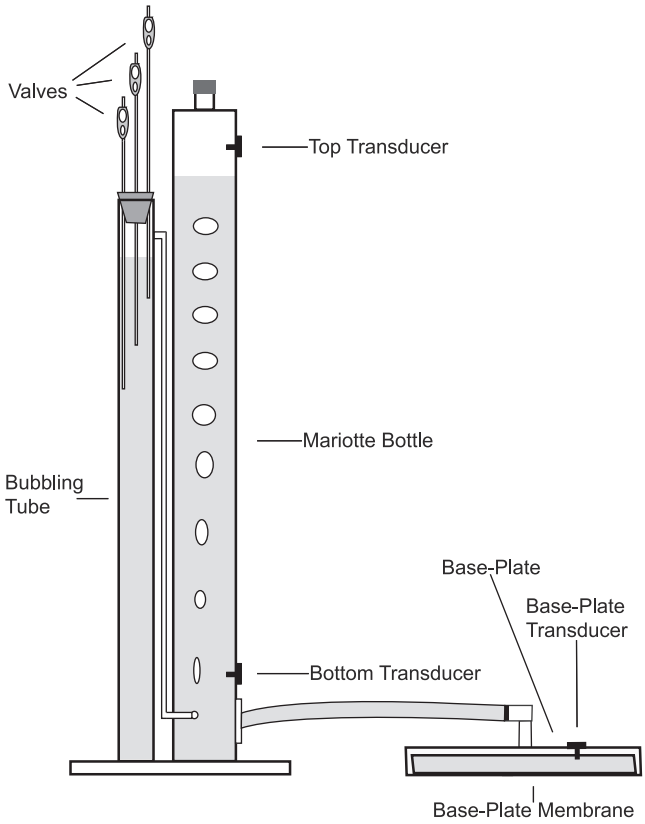

Figure 1. Schematic of the tension infiltrometer. The base plate (on the right) is in contact with the sampled medium. Transducers are used to determine the flux rate from the device and the applied tension at the base plate.

observation errors but adds an inversion model error resulting from poor contact between the disk and the medium. In the following, we discuss our models for observation errors and inversion model errors.

[12] Two sets of observations, each consisting of an applied tension and an observed steady state flux, are required to estimate α and K_s [e.g., *Reynolds and Elrick*, 1991; *Ankeny et al.*, 1991]. We assume that the applied tension is observed using a standard pressure transducer in the base plate (Figure 1). The flux from the Mariotte bottle is estimated by observing the height of water in the bottle with pressure transducers at two different times [e.g., *Ankeny et al.*, 1988]. Observation errors are limited to transducer error and changes in tension due to bubbling within the Mariotte bottle.

[13] The estimated tension, $\hat{\psi}$, at the base plate membrane is expressed as

$$\hat{\psi} = \psi + \xi \tag{3}$$

where ψ is the true tension and ξ is the error due to transducer noise and drift and bubbling error. Because bubbling error is a time dependant phenomena, ξ has a temporal correlation. *Ankeny et al.* [1988] examined this issue and concluded that, in most cases, temporal correlation can be neglected. We assume that ξ is an independent, mean-zero, normally distributed random variable and neglect transducer drift, implying that the transducers themselves are perfectly calibrated. With the assumption of independence, the variance of $\hat{\psi}$ is defined as

$$\sigma^2_{\hat{\psi}} = \frac{\sigma^2_\xi}{M} \tag{4}$$

where σ^2_ξ is the variance of ξ and M is the number of times the transducer is polled. *Ankeny et al.* [1988] reports that the standard deviation of observed pressure within their tension infiltrometer device is 0.62 cm. We assume that this variability is representative of the tension variation at the disk and set $\sigma^2_\xi = 0.4$ cm^2.

[14] Estimates of the flux rate from a tension infiltrometer are most commonly based upon a method described by *Ankeny et al.* [1988]. Two transducers in the Mariotte tube are used to minimize, but not eliminate, the effect of bubbling errors. The flux rate, $\hat{Q}$, is estimated by determining the decline of water-level in the Mariotte tube as infiltration occurs and applying

$$\hat{Q} = \frac{\Delta\hat{H}}{\Delta t}\pi r_t^2 \tag{5}$$

where $\Delta\hat{H} = \hat{H}(t_2) - \hat{H}(t_1)$, $\Delta t = t_2 - t_1$, (the polling interval for the transducers), r_t is the radius of the Mariotte tube, and $\hat{H}(t)$ is the estimated height of the water in the Mariotte tube at time t. Flux errors are caused by errors in estimating the height of the water in the Mariotte tube,

$$\hat{H}(t) = H(t) + \varepsilon \tag{6}$$

where $H(t)$ is the true height of the water in the bubbling tube at time t and ε is an independent, mean-zero, normally distributed error with variance σ^2_ε. As with the error in observed tension, the assumed distribution and assumption of independence of ε is an approximation that improves when the sampling period is much greater than the bubble frequency. If N flux estimates are averaged, then the variance of this estimate is

$$\sigma^2_q = \frac{2\sigma^2_\varepsilon \pi^2 r_t^4}{\Delta t^2 N} \tag{7}$$

We estimate $\sigma^2_\varepsilon = 0.0025$ cm^2 from the results of Figure 2 of *Ankeny et al.* [1988], with spurious data removed. We also assume that the radius of the bubbling tube r_t is 1 cm, that the pressure transducer is polled once per second, and 30 seconds worth of data are averaged to estimate the steady state flux rate. Using (7), the variance of estimated flux rates is $\sigma^2_q = 0.00165$ cm^6/s^2.

[15] We consider only one type of inversion model error, a "contact error" resulting from poor contact between the base plate membrane and the sample medium. It is a common problem during use of the tension infiltrometer and, in our experience, appears to occur more frequently for observations made at higher tensions. This type of error reduces the area for flow and alters the flow geometry. Flaws in the sand contact between the disk and the medium act as large pores, which do not fill at high tensions. At lower tensions, these pores fill, eliminating or reducing the error. Since the tension infiltrometer requires at least two

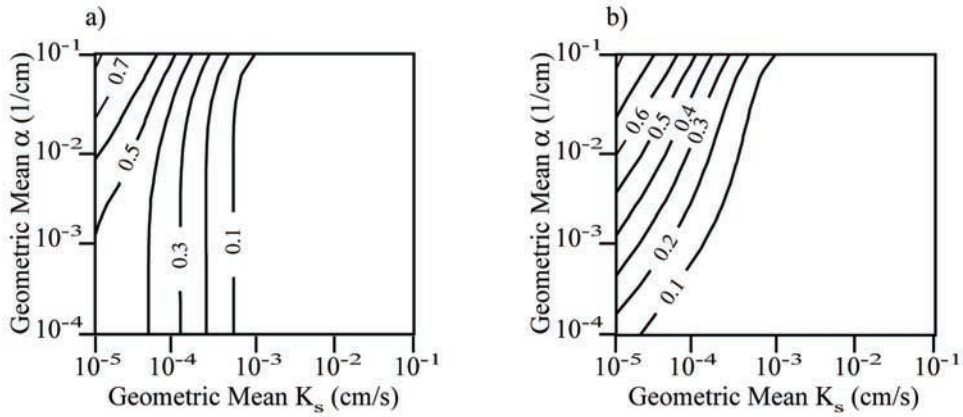

Figure 2. Fraction of points discarded as a function of parameter space with (a) observation error and (b) also with contact error.

observations, one at a higher tension, this error is often more pronounced at the higher tension.

[16] We are not interested in studying contact error in detail, but only its impact on estimating spatial statistics. Consequently, we develop and apply a simple approximation based upon the reduction of area for flow. We assume that the flow geometry does not change and that only the disk area is reduced due to poor contact. We apply this error only at the highest applied tension. The disk area is multiplied by a scaling factor $(1-f)$, where f is selected from a uniform random distribution over 0.0 to 0.1. Because estimates of α and K_s require two flux observations, this error introduces an additional bias in the estimated hydraulic properties. In the following sections, the contact error scenario includes both the contact and observation errors.

2.4. Hydraulic Property Estimates

[17] Using the tension infiltrometer, α and K_s can be estimated from two observed steady state flux measurements, $\hat{Q}_1$ and $\hat{Q}_2$, at the applied tensions $\hat{\psi}_1$ and $\hat{\psi}_2$. We assume that the tension values used for each observation are estimated to be $\hat{\psi}_1 = 2.0$ cm and $\hat{\psi}_2 = 2.0$ cm. These values are selected to insure that ψ_1, which is determined from (3), remains >0.0 cm. The true tensions (ψ_n) are calculated by subtracting ξ from $\hat{\psi}_n$, for n = 1, 2. For each observation, the value of ξ is determined by randomly sampling a mean-zero normal distribution with $\sigma_\xi^2 = 0.4$ cm^2. Given ψ_n, α, and K_s, we calculate the true flux from the tension infiltrometer using [*Wooding*, 1968]

$$Q_n = \frac{K_s}{\alpha} e^{-\alpha\psi_n}\left(\alpha + \frac{4}{\pi r_d}\right)\pi r_d^2 \tag{8}$$

where r_d is the radius of the disk and is equal to 10 cm.

[18] Once the true flux rate is determined, we calculate the estimated flux $\hat{Q}_n$ by adding mean-zero, normally distributed error with $\sigma_q^2 = 0.00165$ cm^6/s^2. At sampling locations where $\hat{Q}_1 \le \hat{Q}_2$ the measurements are discarded, as they would be in practice. Although we and others (e.g., B. P. Mohanty, personal communication, 2000; M. D. Ankeny, personal communication, 2000) have observed and followed this practice in field studies, it is not well documented in the literature. The percentage of discarded points is usually small. For our field studies, it is typically around 5%. In this paper, $\hat{Q}_1 \le \hat{Q}_2$ only because of errors in flux estimates. In field studies, however, inversion model errors, including sub-sample-scale heterogeneity and non-steady state measurements [e.g., *Logsdon*, 1997] may also contribute to this type of error.

[19] When contact errors are considered, $\hat{Q}_1$ is estimated using the procedure outlined above, while $\hat{Q}_2$ is estimated using the same variance σ_q^2 but is estimated using an altered disk radius

$$r_d^* = r_d\sqrt{1-f} \tag{9}$$

where f is sampled from a uniform distribution over 0.0 to 0.1. This means that the disk radius may be reduced from 10 cm to a minimum of ~9.5 cm.

[20] The relative permeability parameter, α, is then estimated with [*Reynolds and Elrick*, 1991]

$$\hat{\alpha} = \frac{\ln(\hat{Q}_1/\hat{Q}_2)}{\hat{\psi}_2 - \hat{\psi}_1} \tag{10}$$

and the saturated hydraulic conductivity, K_s, is estimated with

$$\hat{K}_s = \frac{\hat{\alpha}\hat{Q}_1 e^{\hat{\alpha}\hat{\psi}_1}}{\hat{\alpha}\pi r_d^2 + 4r_d} \tag{11}$$

This procedure is repeated for all pairs of α and K_s values.

2.5. Spatial Statistics

[21] For each spatially correlated random field, the mean, variance, and cross covariance between $\ln(\alpha)$ and $\ln(K_s)$ are determined. In addition, local variograms are calculated for $\ln(\alpha)$, $\ln(K_s)$, $\ln(\hat{\alpha})$, and $\ln(\hat{K}_s)$ using the GSLIB subroutine gam2 [*Deutsch and Journel*, 1998]

$$\gamma(\mathbf{h}) = \frac{1}{2N(\mathbf{h})}\sum_{i=1}^{N(\mathbf{h})}[U(\mathbf{x}_i+\mathbf{h}) - U(\mathbf{x}_i)]^2 \tag{12}$$

where N(**h**) is the number of samples in lag interval **h** and U(x) is the random field. All of the resulting 221 × 4

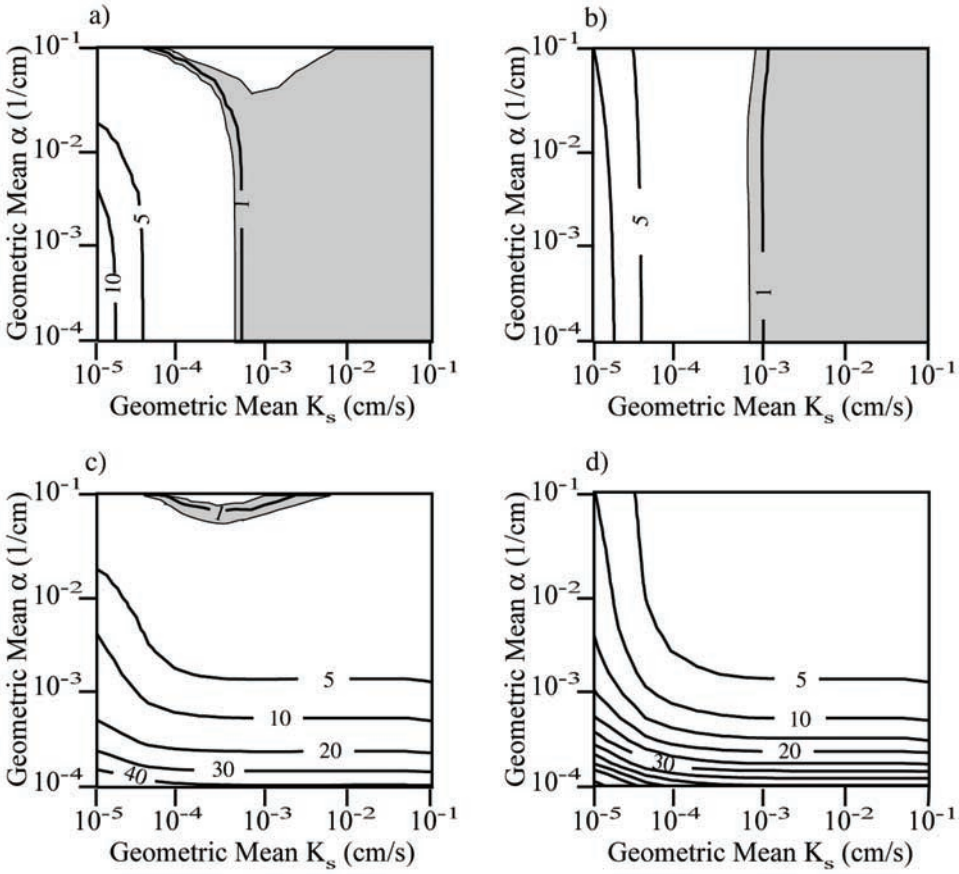

Figure 3. Bias in the geometric mean of (a) $\hat{\alpha}$ and (b) $\hat{K}_s$ estimated with observation errors alone and bias in the geometric mean of (c) $\hat{\alpha}$ and (d) $\hat{K}_s$ estimated with both observation and contact errors. In this and Figures 4–7, bias is shown using a ratio of the "estimated"/"true" value. The bias ratio equals 1.0 for an unbiased statistic and exceeds 1.0 when the estimated statistic is larger than the true statistic. The most accurate region in Figures 3–7, with relative error between 0.95 and 1.05, is shaded.

experimental variograms are fit using a Levenberg-Marquardt algorithm with the exponential variogram model

$$\gamma^m(\mathbf{h}) = \sigma_m^2\left[1 - \exp\left(-\frac{3\mathbf{h}}{\lambda_c}\right)\right] + \sigma_n^2 \qquad (13)$$

where λ_c is the estimated "correlation length", σ_m^2 is the "model variance", and σ_n^2 is the nugget variance. The variance is equal to the sum of the model and nugget variances. When a variogram is constant for all lag distances, we refer to it as a "nugget variogram" in which $\sigma_m^2 = 0.0$ and $\lambda_c = 0.0$. In classical geostatistics, nugget variograms represent white noise processes that have no spatial correlation. To ensure accurate variogram fits, all fitted variograms were visually inspected.

3. Results

[22] Here, we present the results of our Monte Carlo analysis. Our results are plotted as contour maps across the parameter space that is representative of poorly-sorted to well-sorted silt to coarse sand. We first consider the fraction of points discarded because of a physically implausible result, $\hat{Q}_1 \leq \hat{Q}_2$. We then present the bias in the mean, variance, and variogram model parameters for $\ln(\hat{\alpha})$ and $\ln(\hat{K}_s)$ across our parameter space. We also show that measurement errors can introduce false cross correlation between $\ln(\hat{\alpha})$ and $\ln(\hat{K}_s)$. Finally, we discuss our results at the end of the section. In the following, bias for statistical parameters is shown using a ratio of "estimated"/"true" value. The bias ratio equals 1.0 for an unbiased statistic and exceeds 1.0 when the estimated statistic is larger than the true statistic.

[23] Figures 2a and 2b show the fraction of points discarded (FPD) because of an unrealistic result, $\hat{Q}_1 \leq \hat{Q}_2$. The FPD increases when tension infiltrometer flux rates are small and errors dominate flux rate measurements. This occurs when α is high and K_s is small. When only observation errors are considered (Figure 2a), the FPD is larger than when contact errors are included (Figure 2b). When contact errors are present, the FPD decreases across the parameter space because $\hat{Q}_2$ is underestimated, reducing the likelihood that $\hat{Q}_1 \leq \hat{Q}_2$. The rejection of points introduces a bias in the flux values at the remaining points. Points are more likely to be discarded when either $\hat{Q}_1$ is too small or $\hat{Q}_2$ is too large. At retained points, $\hat{Q}_1$ measurements tend to be high while $\hat{Q}_2$ measurements tend to be low. This bias in flux rates affects the spatial statistics of $\ln(\hat{\alpha})$ and $\ln(\hat{K}_s)$. It is important to note that property bias also results from the propagation of unbiased observation errors through the inversion model, as we'll see next.

[24] Figure 3 presents errors in the geometric means of estimated properties $\hat{\alpha}$ and $\hat{K}_s$. The most accurate region in

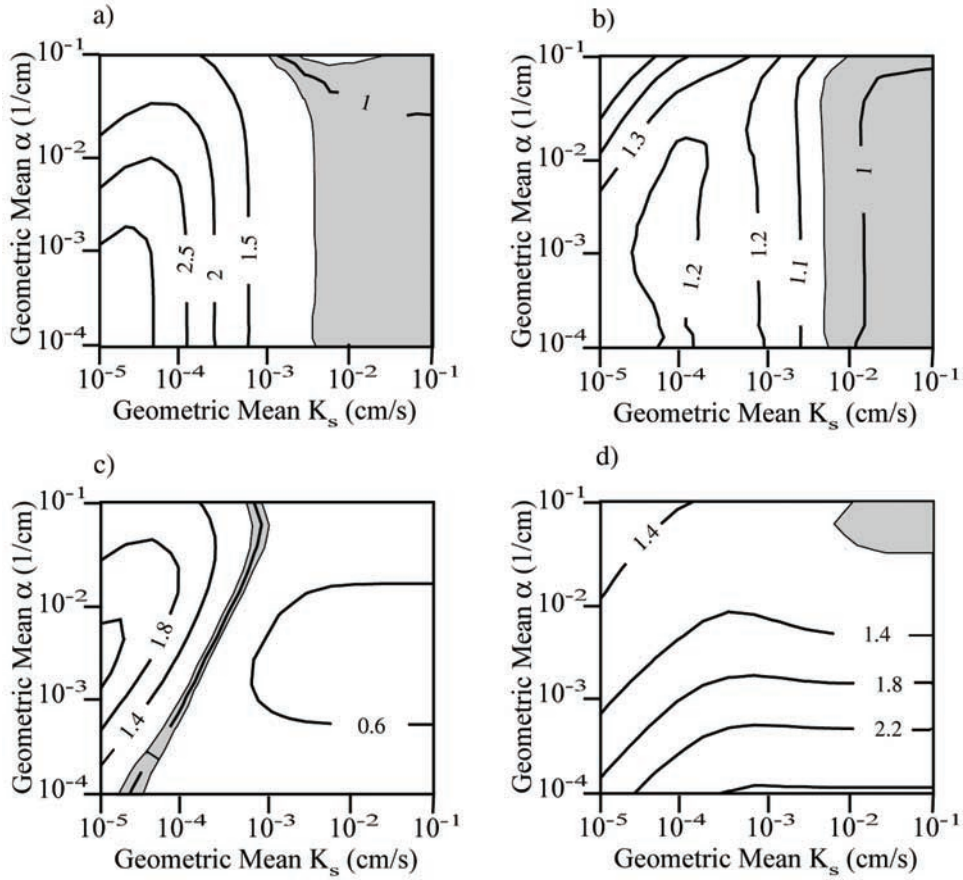

Figure 4. Bias in the variance of (a) $\ln(\hat{\alpha})$ and (b) $\ln(\hat{K}_s)$ estimated with observation errors alone and bias in the variance of (c) $\ln(\hat{\alpha})$ and (d) $\ln(\hat{K}_s)$ estimated with both observation and contact errors.

this and the following figures, with a bias ratio between 0.95 and 1.05, is shaded. When only observation errors are present (Figures 3a and 3b), the geometric means of both properties are accurately estimated in an overlapping region characterized by high mean hydraulic conductivity (i.e., flux rates are high relative to flux rate errors). The geometric means show greater bias when the mean hydraulic conductivity is small (i.e., flux rates are small). Bias in the geometric mean of $\hat{\alpha}$ also decreases at high α^G where the FPD (Figure 2a) is greatest. This is counterintuitive because a large FPD indicates that the flux rates, $\hat{Q}_1$ and $\hat{Q}_2$, are strongly biased. However, bias in the log flux ratio, $\ln(\hat{Q}_1/\hat{Q}_2)$ from (10), decreases at high α^G and increases at low α^G. This result shows that bias in an estimated property may not reflect the bias in the observations.

[25] Figures 3c and 3d show that the biases in the geometric means change drastically when contact error is added. The geometric mean $\hat{\alpha}$ is only accurately estimated in a narrow region near the top of parameter space (high α^G), while the geometric mean $\hat{K}_s$ is overestimated across the entire parameter space. In contrast to the observation-error case, estimated geometric means show strong dependence on α^G. Contact errors decrease $\hat{Q}_2$, leading to an increase in the flux ratio and overestimation of both $\hat{\alpha}$ and $\hat{K}_s$.

[26] Figure 4 shows bias in the variance of $\ln(\hat{\alpha})$ and $\ln(\hat{K}_s)$. When only observation errors are present (Figures 4a and 4b), errors in the variance of both parameters appear similar except that the variance of $\ln(\hat{\alpha})$ is larger. The variance of $\ln(\hat{\alpha})$ and $\ln(\hat{K}_s)$ is accurately estimated at large hydraulic conductivity. Errors increase as α^G and K_s^G decreases, except at very small hydraulic conductivity (far left portion of parameter space) where the errors decrease again. As α^G or K_s^G decreases, the variability of the log ratio in (10) increases, increasing the variance of $\ln(\hat{\alpha})$. At very small K_s^G, however, $\hat{Q}_1$ and $\hat{Q}_2$ are dominated by errors. The variability of the log ratio is reduced, and the variance of $\ln(\hat{\alpha})$ decreases.

[27] Figures 4c and 4d show that the errors in the variance of $\ln(\hat{\alpha})$ and $\ln(\hat{K}_s)$ change significantly when contact errors are added. Accurate regions are much smaller for both $\ln(\hat{\alpha})$ and $\ln(\hat{K}_s)$, and they no longer overlap. Errors in the variances of $\ln(\hat{\alpha})$ and $\ln(\hat{K}_s)$ show greater dependence on α^G. The variance of $\ln(\hat{\alpha})$ is underestimated across much of the parameter space, because $\hat{Q}_2$ becomes independent of $\hat{Q}_1$ when contact errors are present. The variance of $\ln(\hat{K}_s)$ is overestimated at low α^G because of compensating errors. Consider the covariance between $\hat{Q}_1$ and $\hat{\alpha}$ in

$$\mathrm{var}\left[\ln(\hat{K}_s)\right] \propto \mathrm{var}[\ln(\hat{\alpha})] + \mathrm{var}\left[\ln(\hat{Q}_1)\right] + 2\mathrm{cov}\left[\ln(\hat{\alpha}), \ln(\hat{Q}_1)\right] \tag{14}$$

In general, $\ln(\hat{Q}_1)$ and $\ln(\hat{\alpha})$ exhibit a large negative covariance that reduces the variance of $\ln(\hat{K}_s)$. When contact errors are present, however, this covariance approaches zero because $\hat{\alpha}$ depends primarily on the errors in $\hat{Q}_2$.

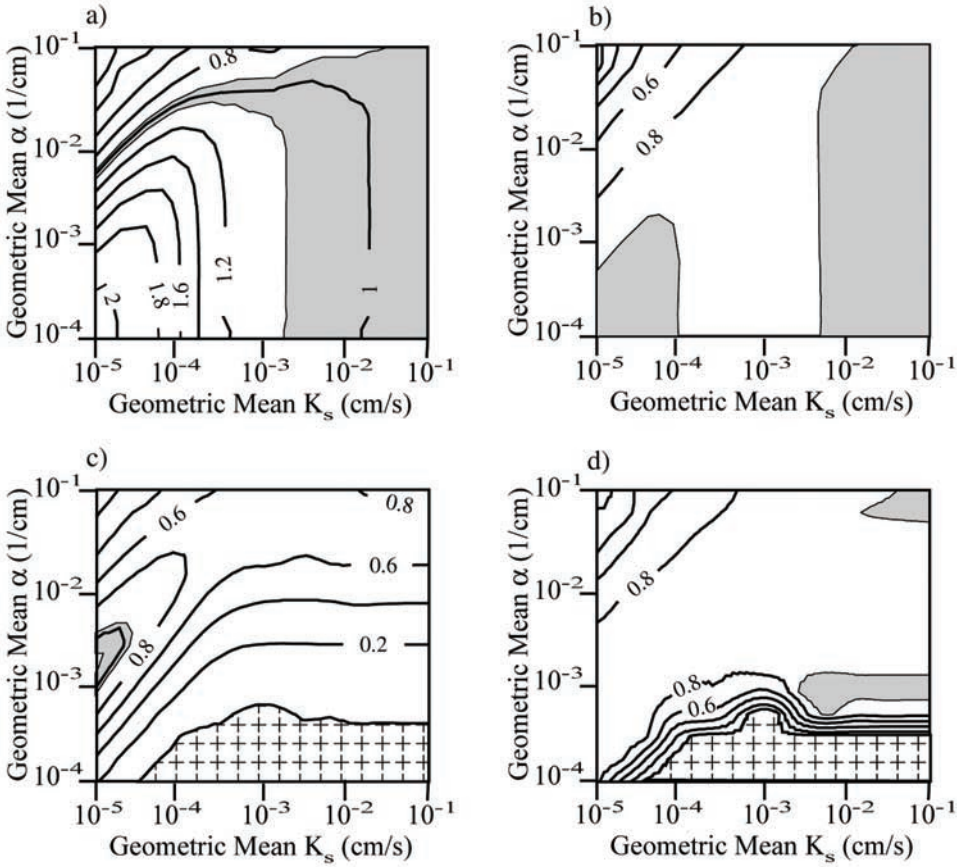

Figure 5. Bias ratio for variogram model parameters of $\ln(\hat{\alpha})$: (a) model variance with measurement errors only, (b) correlation length with measurement error only, (c) model variance with contact error, and (d) correlation length with contact error. Regions equal to zero are patterned, indicating nugget variograms, in this figure and Figure 6.

[28] Bias in the variogram model variance and correlation length for $\ln(\hat{\alpha})$ is shown in Figures 5a and 5b, respectively. Both the model variance and correlation length are accurately estimated at large K_s^G. The pattern of error in the model variance is similar to the pattern of error in the variance of $\ln(\hat{\alpha})$ (Figure 4a), except in the upper left corner of parameter space (high α^G and small K_s^G) where the model variance approaches zero. Correlation lengths are accurately estimated, with bias values near one, across most of the parameter space. As with the model variance, correlation lengths become inaccurate in the upper left corner of parameter space (Figure 5b).

[29] Figures 5c and 5d display the bias in the model variance and correlation length for $\ln(\hat{\alpha})$ when contact errors are added. Regions equal to zero are patterned indicating nugget variograms in these and all remaining figures. There are no overlapping accurate regions, and nugget variograms (model variance and correlation length equal to 0.0) result at low α^G. Unlike the variance (Figure 4c), the model variance is underestimated across the entire parameter space. The correlation length, however, is more accurate with a bias ratio >0.8 across most of parameter space. At low α^G, noise due to random contact errors eliminates spatial correlation leading to nugget variograms.

[30] Figures 6a and 6b present the bias in the model variance and correlation length for $\ln(\hat{K}_s)$. Model variances and correlation lengths are accurately estimated across much of the parameter space. Nugget variograms occur at small K_s^G and low α^G. The pattern of error in the model variance of $\ln(\hat{K}_s)$ differs greatly from that of the variance of $\ln(\hat{K}_s)$ (Figure 4b), which is overestimated in this region. The variogram of $\ln(\hat{K}_s)$ is

$$\gamma_{\ln(\hat{K}_s)} \propto \gamma_{\ln(\hat{\alpha})} + \gamma_{\ln(\hat{Q}_1)} + 2\gamma_{\ln(\hat{\alpha}),\ln(\hat{Q}_1)} \tag{15}$$

where $\gamma_{\ln(\hat{\alpha})}$ is the variogram of $\ln(\hat{\alpha})$, $\gamma_{\ln(\hat{Q}_1)}$ is the variogram of $\ln(\hat{Q}_1)$, and $\gamma_{\ln(\hat{\alpha}),\ln(\hat{Q}_1)}$ is the cross-variogram between $\ln(\hat{\alpha})$ and $\ln(\hat{Q}_1)$. At small K_s^G and low α^G, $\gamma_{\ln(\hat{\alpha})}$ is large (Figures 5a and 5b), but noise from error in the flux rates cause $\gamma_{\ln(\hat{Q}_1)}$ to be underestimated. $\gamma_{\ln(\hat{\alpha}),\ln(\hat{Q}_1)}$ maintains large negative values, reducing the relative contribution from $\gamma_{\ln(\hat{\alpha})}$.

[31] When contact error is added, patterns of bias in the model variance and correlation length of $\ln(\hat{K}_s)$ change (Figures 6c and 6d). Accurate regions for the model variance and correlation length do not over lap. The model variance is overestimated, but the correlation length remains fairly accurate (bias ratio >0.8) across most of the parameter space. Errors in the cross-variogram $\gamma_{\ln(\hat{\alpha}),\ln(\hat{Q}_1)}$ still strongly control the variogram of $\ln(\hat{K}_s)$. At low α^G, $\ln(\hat{\alpha})$ is controlled by errors in $\hat{Q}_2$, and $\gamma_{\ln(\hat{\alpha}),\ln(\hat{Q}_1)}$ is small. As a result, the estimated correlation length of $\ln(\hat{K}_s)$ is fairly accurate (Figure 6d), but the model variance is greatly overestimated (Figure 6c). As with the case with no contact error, model variances and correlation lengths approach zero

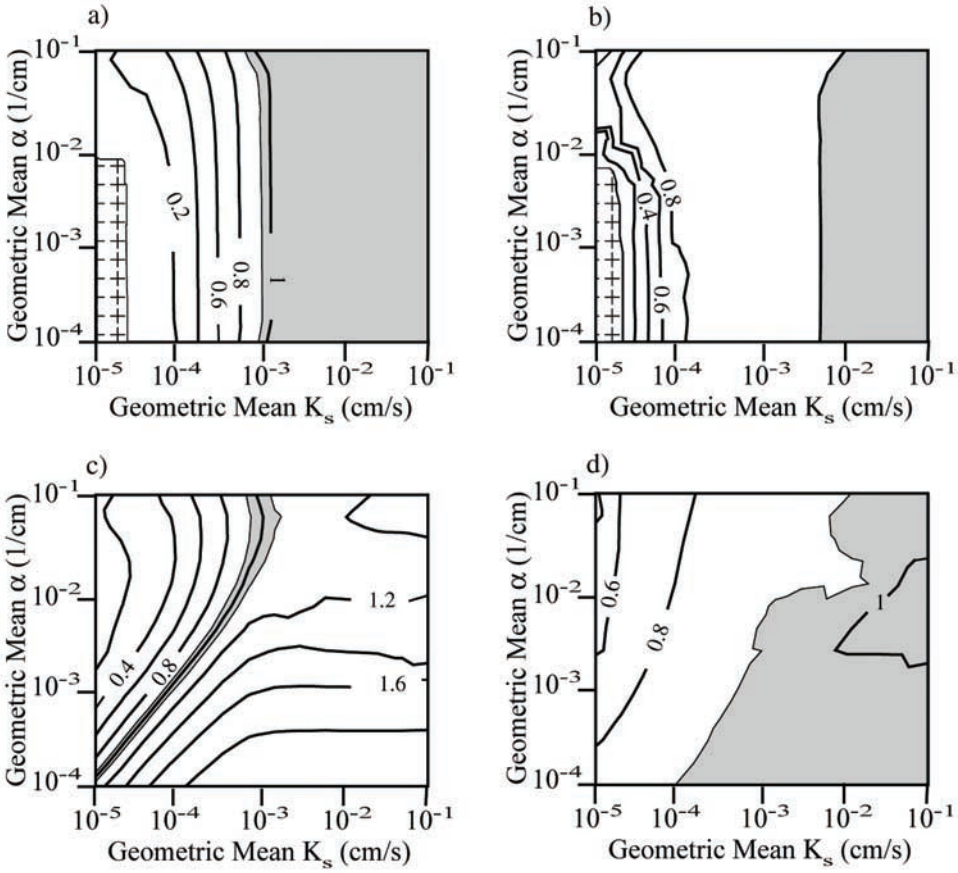

Figure 6. Bias ratio for variogram model parameters of $\ln(\hat{K}_s)$: (a) model variance with measurement errors only, (b) correlation length with measurement error only, (c) model variance with contact error, and (d) correlation length with contact error.

at high α^G and small K_s^G (upper left corner), because flux rate estimates are dominated by errors.

[32] Although true properties $\ln(\alpha)$ and $\ln(K_s)$ are statistically independent, we observe significant cross correlation between estimated properties $\ln(\hat{\alpha})$ and $\ln(\hat{K}_s)$ (Figure 7). False cross correlation between $\ln(\hat{\alpha})$ and $\ln(\hat{K}_s)$ results because both $\hat{\alpha}$ and $\hat{K}_s$ depend on $\hat{Q}_1$ ((10) and (11)), and $\hat{K}_s$ depends on and increases with $\hat{\alpha}$ (equation (11)), yielding positive point correlation functions. When only measurement errors are present, the correlation coefficient for $\ln(\hat{\alpha})$ and $\ln(\hat{K}_s)$ appears to increase as K_s^G decreases, reflecting increasing errors in the flux rates. When contact errors are added, the pattern of the correlation coefficient changes, and strong cross correlation is observed at both large K_s^G and

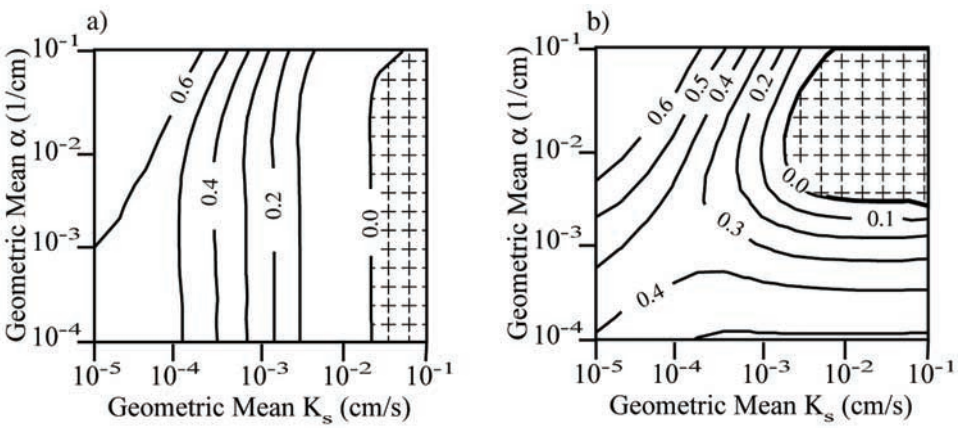

Figure 7. Correlation coefficients for $\ln(\hat{\alpha})$ and $\ln(\hat{K}_s)$ as a function of parameter space: (a) with measurement error only and (b) also with contact error. Regions with correlation coefficients equal to zero are patterned.

low α^G (lower right corner), and small K_s^G and high α^G (upper left corner of parameter space). This occurs because $\hat{\alpha}$ tends to be overestimated in this region of parameter space (Figure 3c).

4. Discussion

[33] Bias in the spatial statistics of $\ln(\hat{\alpha})$ and $\ln(\hat{K}_s)$ results from the propagation of small, simple observation and inversion model errors through nonlinear inversion models, equations (10) and (11). For both parameters, the magnitude of bias varies with the "true" spatial statistics of the underlying field (i.e., the mean). Our results also show that bias in spatial statistics may not follow bias in observations (i.e., the FPD), due to nonlinearity in the inversion model. The inversion model filters biased observations and can lead to counterintuitive property errors when nonlinearity is strong. Empirical models for the variance and variogram are also nonlinear filters. As a result, variogram or variance bias may be significantly different from bias in the mean. The character of bias changes between one-point and two-point statistics (e.g., the variance and the variogram) because errors are random space functions characterized by their own variogram. Finally, our results show that observation and inversion model errors can lead to erroneous cross correlation between parameters.

[34] Bias in spatial statistics varies greatly depending upon the type of error affecting measurements. Our results show that when only observation errors affect property measurements overlapping accurate regions for all spatial statistics occur somewhere in parameter space. Inversion model errors, however, are much more insidious because overlapping accurate regions do not occur. In principle, observation errors can be limited by design. It is almost impossible, however, to eliminate inversion model errors because inversion models cannot incorporate all the physics relevant to a hydraulic property [*Beckie*, 1996].

[35] In this study, points are discarded when measurement errors produce unrealistic results. Contact error, an inversion model error, actually increases the number of interpretable data, but does not improve the spatial statistics of $\ln(\hat{\alpha})$ and $\ln(\hat{K}_s)$. In practice, data that are spurious, unrealistic, or difficult to interpret are routinely discarded, possibly contributing to bias in hydraulic property estimates. Conversely, one cannot infer that apparently good data implies no bias in property estimates, because biased properties can result from the propagation of unbiased observation error through a nonlinear inversion model.

[36] Unfortunately, we find no unique indicators of bias in tension infiltrometer data. Certain results (e.g., large FPD, large positive correlation coefficients, and nugget variograms) can strongly suggest the presence of bias, but indicators of little or no bias are not obvious from our results. The spatial statistics (mean, variance, and variogram) offer few diagnostic indicators of measurement bias. In fact, spatial statistics can appear realistic, but still be strongly biased. Nugget variograms could indicate either strong bias or lack of spatial correlation. Similarly a nugget effect in the variogram, a positive difference between the variance and model variance, could indicate bias but may also indicate uncorrelated random errors, sub-sample scale heterogeneity, or nonideal sample location [e.g., *Journel and Huijbregts*, 1978].

5. Neglected Errors

[37] In this illustrative study we include only very small and simple forms of error and neglect many other types of error likely to affect tension infiltrometer measurements. Consequently, the spatial statistics of field-estimated properties are likely to show more bias than that reported here.

[38] Observation errors may be larger than those used for this study. The flux rate errors used here were based on instrument observations reported by *Ankeny et al.* [1988]. Their observations were made under highly controlled laboratory conditions (M. D. Ankeny, personal communication, 1998). We conducted a series of laboratory repeatability studies to evaluate directly the flux rate variance, σ_q^2, during realistic tension infiltrometer operation. A large sandbox was constructed and filled with well-sorted, fine sand. The tension infiltrometer (manufactured by Soil Measurement Systems of Tucson, Arizona) was calibrated using standard methods [e.g., *Soil Measurement Systems*, 1992], and applied following normal procedures. After each test, the sand was returned to a constant initial condition by applying a vacuum to a pressure plate at the base of the box. For these tests, σ_q^2 was determined to be 0.06 cm^6/s^2. This value may be more representative of field studies than the flux-error variance used here (σ_q^2 = 0.00165 cm^6/s^2).

[39] Errors in applied tension at the disk source may also be much larger than considered here. Many tension infiltrometers do not have a pressure transducer located at the disk source. Instead the applied tension at the disk is traditionally calibrated at a given bubble rate [e.g., *Soil Measurement Systems*, 1992]. A constant bubble rate is achieved by establishing a vacuum on the Mariotte bottle, and a manometer is connected to the source tube for the disk. The depth of the air entry tubes is adjusted until the desired tension in the source tube is reached. This approach, however, is subject to a variety of errors. Because temperature changes will affect the expansion of bubbles, effective steady state tensions will systematically vary from the calibrated values. In addition, some tension infiltrometers have a separate disk, and errors will be introduced if the disk is not at the correct elevation relative to the Mariotte bottle.

[40] In this study, we included only one simple inversion model error, that due to poor contact with the sampled medium. Other inversion model errors can also produce biased spatial statistics. These other potential sources of bias include sub-sample-scale heterogeneity, viscosity variations, changes in the medium during infiltration, soils with nonexponential hydraulic conductivity functions, and air entrapment.

6. Summary and Implications

[41] We use Monte Carlo error analyses to illustrate the impact of observation and inversion model errors on the spatial statistics determined from field-measured unsaturated hydraulic properties. We construct a series of idealized artificial realities (spatially correlated random fields) completely described by the Gardner parametric model [*Gard-*

ner, 1958]. We assume that parameters α and K_s are lognormally distributed random fields completely characterized by their geometric means and exponential variograms. The geometric means (α^G and K_s^G) are varied between 221 different realities to reveal the connection between true property values and errors in spatial statistics. Geometric means are selected to represent a parameter space that varies from poorly sorted to well-sorted, silt to coarse sand. Properties are estimated using simulated tension infiltrometer measurements subject to small, simple errors. To minimize the degrees of freedom in our problem, we consider two error scenarios. The first is an observation-error scenario with errors in estimates of tension infiltrometer flux rates and applied pressures at the disk source. The second is a contact-error (inversion model error) scenario that adds a boundary-condition error due to poor contact between the tension infiltrometer disk and the sampled medium. The spatial statistics (mean, variance, correlation length, and variogram model variance) of the true and estimated property fields are determined using all locations within each reality to insure that errors in spatial statistics reflect only errors in property measurements.

[42] Our results show that even in very idealized, simplified systems small observation and inversion model errors can lead to significant bias in the spatial statistics of measured hydraulic properties. We discard data locations due to a physically implausible result, $\hat{Q}_1 \leq \hat{Q}_2$. The fraction of discarded points, FPD, increases in that part of parameter space characterized by low flux rates (high α^G and small K_s^G), and decreases when contact errors are present. Errors in statistics, however, tend not to be controlled by the fraction of discarded points because the inversion model filters bias in observations and our inversion model errors are independent of observations. When only observation errors are present, spatial statistics for $\ln(\hat{\alpha})$ and $\ln(\hat{K}_s)$ are accurately estimated in overlapping regions at large K_s^G. With the addition of our inversion model error, however, the error patterns change significantly and accurate regions do not overlap. The magnitude and pattern of error vary for different spatial statistics, so that knowledge of bias for one statistical measure is of limited use in predicting bias in another. Although we generated uncorrelated fields of $\ln(\alpha)$ and $\ln(K_s)$, we observe significant correlation between $\ln(\hat{\alpha})$ and $\ln(\hat{K}_s)$ indicating that observation and inversion model errors can generate artificial cross correlation between parameters.

[43] These findings have broad implications for instruments used for characterizing spatial variability. Observation and inversion model errors lead to biased estimates of hydraulic properties and their spatial statistics when inversion models are nonlinear. Bias is most sensitive to inversion model errors because observation errors are minimized by design. Bias is not homogeneous, and its extent of bias depends on the character of the measured statistic, inversion model nonlinearity, the true values of the sampled hydraulic properties, and the nature of observation and inversion model errors affecting measurements. Strong bias can produce or eliminate cross correlation between parameters and preclude accurate estimation of the mean, variance, and variogram. The effects of observation and inversion model error can be insidious, as hydraulic property estimates may appear reasonable and generate realistic-looking spatial statistics which are, however, inaccurate and misleading. The geostatistical approaches used in spatial variability studies offer no formal approaches for detecting and treating measurement bias.

[44] We've identified three different audiences for this paper. First, most geostatisticians do not consider how measurement noise and inversion errors bias spatial statistics, except to roughly approximate it through a nugget term. This paper illustrates that that naivete can produce misleading results. Unfortunately there is no simple diagnostic to identify the presence of this bias, nor is there a filter to remove it. It remains an area of open investigation that depends on the instrument and what it measures. Vadose zone stochastic flow and transport modelers compose the second audience. They seek spatial statistics to parameterize their models. The presence of significant parameter bias suggests that, by using these biased parameter estimates, their predictions should also be biased, perhaps seriously. The last audience is composed of instrumentation practitioners, particularly those who employ the tension infiltrometer or related unsaturated zone instruments. In recent years it has become increasingly evident that a major application of these instruments is for geostatistical and stochastic studies, raising the concerns expressed above. But this paper also suggests more traditional concerns for these instruments. Instruments employing sufficiently nonlinear inversions may not be able to distinguish subtle differences between materials.

[45] **Acknowledgments.** This research was supported by the U. S. Department of Energy's Environmental Management Science Program (EMSP) under contract numbers DE-FG07-96ER14704 (New Mexico Institute of Mining and Technology) and DE-AC04-94AL85000 (Sandia National Laboratories). Tension infiltrometer experiments were performed at the Flow Visualization and Processes Laboratory at Sandia National Laboratories, and we thank Martha Whitaker for her help with this work. We also thank Sean McKenna and Jan Hendrickx for their reviews of an earlier version of this manuscript. We are especially grateful to Allan Gutjahr for his contributions in the early part of this work and reviews of early versions of this manuscript. Finally, we are grateful to David Rogers and two anonymous reviewers. Their comments helped to improve this manuscript.

References

Ankeny, M. D., T. C. Kaspar, and R. Horton, Design for an automated tension infiltrometer, *Soil Sci. Soc. Am. J.*, *52*, 893–896, 1988.

Ankeny, M. D., M. Ahmed, T. C. Kaspar, and R. Horton, Simple field method for determining unsaturated hydraulic conductivity, *Soil Sci. Soc. Am. J.*, *55*, 467–470, 1991.

Beckie, R., Measurement scale, network sampling scale, and groundwater model parameters, *Water Resour. Res.*, *32*(1), 65–76, 1996.

Bresler, E., Analysis of trickle irrigation systems with application to design problems, *Irrig. Sci.*, *1*, 3–17, 1978.

Clothier, B. E., D. Scotter, and E. Harper, Three-dimensional infiltration and trickle irrigation, *Trans. Am. Soc. Agric. Eng.*, *28*, 497–501, 1985.

Deutsch, C. V., and A. G. Journel, *GSLIB*: *Geostatistical Software Library and User's Guide*, 2nd ed., Oxford Univ. Press, New York, 1998.

Freeze, R. A., and J. A. Cherry, *Groundwater*, Prentice-Hall, Englewood Cliffs, N. J., 1979.

Gardner, W. R., Some steady state solutions of unsaturated moisture flow equations with application to evaporation for a water table, *Soil Sci.*, *85*, 228–232, 1958.

Hussen, A. A., and A. W. Warrick, Alternative analyses of hydraulic data from disc tension infiltrometers, *Water Resour. Res.*, *29*(12), 4103–4108, 1993.

Indelman, P., D. Or, and Y. Rubin, Stochastic analysis of unsaturated steady state flow through bounded heterogeneous formations, *Water Resour. Res.*, *29*(4), 1141–1148, 1993.

Istok, J. D., D. O. Blout, L. Barker, K. R. Johnejack, and D. P. Hammermeister, Spatial variability in alluvium properties at a low-level nuclear waste site, *Soil Sci. Soc. Am. J.*, *58*, 1040–1051, 1994.

Jarvis, N. J., and I. Messing, Near-saturated hydraulic conductivity in soils of contrasting texture measured by tension infiltrometers, *Soil Sci. Soc. Am. J.*, *59*, 27–34, 1995.

Journel, A. G., and C. J. Huijbregts, *Mining Geostatistics*, Academic, San Diego, Calif., 1978.

Kempthorne, O., and R. R. Allmaras, Errors and variability of observations, in *Methods of Soil Analysis*, part 1, *Physical and Mineralogical Methods*, 2nd ed., edited by A. Klute, pp. 1–31, Am. Soc. of Agron., Madison, Wis., 1986.

Logsdon, S. D., Transient variation in the infiltration rate during measurement with tension infiltrometers, *Soil Sci.*, *162*, 233–241, 1997.

Mandel, J., *The Statistical Analysis of Experimental Data*, Dover, Mineola, N. Y., 1964.

Mantoglou, A., and L. W. Gelhar, Capillary tension head variance, mean soil moisture content, and effective specific soil moisture capacity of transient unsaturated flow in stratified soils, *Water Resour. Res.*, *23*(1), 47–56, 1987a.

Mantoglou, A., and L. W. Gelhar, Effective hydraulic conductivities of transient unsaturated flow in stratified soils, *Water Resour. Res.*, *23*(1), 57–67, 1987b.

Mohanty, B. P., M. D. Ankeny, R. Horton, and R. S. Kanwar, Spatial analysis of hydraulic conductivity measured using disc infiltrometers, *Water Resour. Res.*, *30*(9), 2489–2498, 1994.

Philip, J. R., Theory of infiltration, *Adv. Hydrosci.*, *5*, 215–296, 1969.

Reynolds, W. D., and D. W. Elrick, A laboratory and numerical assessment of the Guelph permeameter method, *Soil Sci.*, *144*, 282–299, 1987.

Reynolds, W. D., and D. W. Elrick, Determination of hydraulic conductivity using a tension infiltrometer, *Soil Sci. Soc. Am. J.*, *55*(3), 633–639, 1991.

Robin, M. J. L., A. L. Gutjahr, E. A. Sudicky, and J. L. Wilson, Cross-correlated random field generation with the direct Fourier transform method, *Water Resour. Res.*, *29*(7), 2385–2397, 1993.

Russo, D., and M. Bouton, Statistical analysis of spatial variability in unsaturated flow parameters, *Water Resour. Res.*, *28*(7), 1911–1925, 1992.

Russo, D., I. Russo, and A. Laufer, On the spatial variability of parameters of the unsaturated hydraulic conductivity, *Water Resour. Res.*, *33*(5), 947–956, 1997.

Shouse, P. J., and B. P. Mohanty, Scaling of near-saturated hydraulic conductivity measured using disc infiltrometers, *Water Resour. Res.*, *34*(5), 1195–1205, 1998.

Simunek, J., and M. T. van Genuchten, Estimating unsaturated soil hydraulic properties from tension disc infiltrometer data by numerical inversion, *Water Resour. Res.*, *32*(9), 2683–2696, 1996.

Soil Measurement Systems, Tension infiltrometer users manual, Tucson, Ariz., 1992.

U.S. Department of Energy (U.S. DOE), Hydrogeologic data for existing excavations at the Area 5 Radioactive Waste Management site, Nevada Test Site, Nye County, Nevada, *DOE/NV/11432-40*, U.S. Dep. of Energy Nev. Operations Off., Las Vegas, 1993.

White, I., and M. J. Sully, On the variability and use of the hydraulic conductivity alpha parameter in stochastic treatments of unsaturated flow, *Water Resour. Res.*, *28*(1), 209–213, 1992.

Wooding, R. A., Steady infiltration from a shallow circular pond, *Water Resour. Res.*, *4*(6), 1259–1273, 1968.

Yeh, T.-C. J., L. W. Gelhar, and A. L. Gutjahr, Stochastic analysis of unsaturated flow in heterogeneous soils, 1, Statistically isotropic media, *Water Resour. Res.*, *21*(4), 447–456, 1985a.

Yeh, T.-C. J., L. W. Gelhar, and A. L. Gutjahr, Stochastic analysis of unsaturated flow in heterogeneous soils, 2, Statistically isotropic media with variable α, *Water Resour. Res.*, *21*(4), 457–464, 1985b.

Yeh, T.-C. J., L. W. Gelhar, and A. L. Gutjahr, Stochastic analysis of unsaturated flow in heterogeneous soils, 3, Observations and applications, *Water Resour. Res.*, *21*(4), 465–471, 1985c.

Zhang, D. Z., T. C. Wallstrom, and C. L. Winter, Stochastic analysis of steady-state unsaturated flow in heterogeneous media: Comparison of the Brooks-Corey and Gardner-Russo models, *Water Resour. Res.*, *34*(6), 1437–1449, 1998.

R. J. Glass, Flow Visualization and Processes Laboratory, Sandia National Laboratories, Albuquerque, NM 87185, USA.

R. M. Holt, Department of Geology and Geological Engineering, University of Mississippi, University, MS 38677, USA. (rmholt@olemiss.edu)

J. L. Wilson, Department of Earth and Environmental Sciences, New Mexico Institute of Mining and Technology, Socorro, NM 87801, USA.